LANGMUIR

pubs.acs.org/Langmuir Article

Interfacial Density Profiles of Polar and Nonpolar Liquids at Hydrophobic Surfaces

Miaoqi Chu, Mitchell Miller, and Pulak Dutta*

Cite This: *Langmuir* 2020, 36, 906−910 Read Online

ACCESS | Metrics & More | Article Recommendations | Supporting Information

A density-depleted region ("gap") is known to exist between water and hydrophobic surfaces. Using X-ray reflectivity, we have observed similar gaps between hydrophobic self-assembled monolayers (SAMs) and four other polar liquids. For these liquids and for water, the observed electron density depletion is nonzero and is in most cases slightly greater than the depletion attributable to the layer of hydrogen atoms at the SAM surface. On the other hand, the observed X-ray reflectivity from the interfaces between SAMs and three nonpolar liquids studied can be explained either without gaps or with smaller gaps. Thus, polar liquids (including but not limited to water) stand away from even the terminal hydrogen atoms at hydrophobic surfaces, while nonpolar liquids interpenetrate the terminal region. There is no consistent correlation between the sizes of the gaps and the liquid−SAM contact angles, the relative polarities of the polar liquids, or their bulk densities.

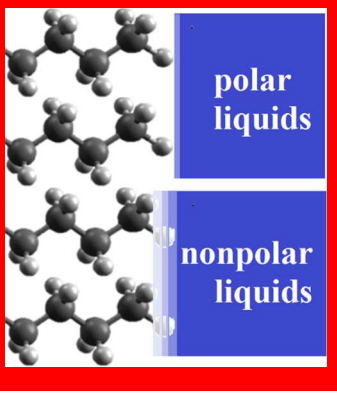

INTRODUCTION

How does a liquid make contact with a solid surface? The profile of a solid−liquid interface is relevant to many real-world processes and applications such as lubrication, chemical reactions, drug delivery, coating adhesion, and labs-on-a-chip. In particular, the interface between water and hydrophobic surfaces has been the subject of much theoretical and experimental attention.[1−10]

Unfortunately, while theory and simulations have produced very detailed predictions regarding liquid−solid interface profiles, empirical verification has not been as easy. Although there are spectroscopic methods sensitive enough to detect molecular orientation and bonding at interfaces,[11] there is no probe other than synchrotron X-ray reflectivity (XRR) that approaches the sub-nanoscale resolution necessary to determine interfacial density profiles. (Neutron reflectivity is in principle similar, but neutron beams have much lower usable intensities and therefore poorer spatial resolution.[8]) However, even with XRR, deviations from the bulk electron density near a solid−liquid interface are always close to the limit of detection. Therefore, the customary way to simplify the problem is to represent the interfacial density anomalies as square wells or "gaps" (see Figure 1). This does not mean that the interfacial profile actually has a "square well" form; one merely approximates the gap with a simple shape ("parsimony") since experimental accuracy does not justify a more complicated model function. The gap is described by two parameters, the gap width D_g and the gap density ρ_g (see Figure 1). One can also define a combined parameter $D_{eq} \equiv D_g(\rho_L-\rho_g)/\rho_L$, where ρ_L is the electron density of the bulk liquid. This is the effective width of the gap, in other words, the width of a gap that has the same integrated density depletion but zero-gap density. (The importance of D_{eq} will be discussed in detail further below in this paper.)

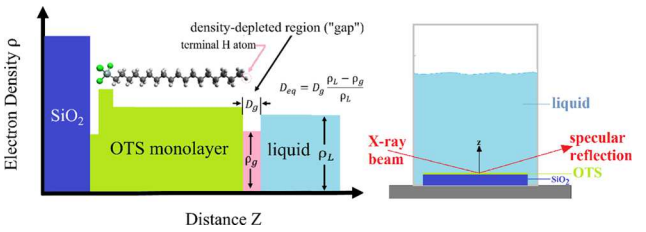

Figure 1. LEFT: The box model interfacial density profile used to fit the XRR data at the liquid−self-assembled monolayer (SAM) interfaces. The interfaces are shown in the figure as sharp steps for clarity, but in the actual data analysis are rounded using error functions. Note that the SiO_2 layer at the far left and the liquid layer at the far right are modeled as semi-infinite slabs because they are much thicker than the photon coherence length. RIGHT: Schematic diagram showing the geometry of the XRR experiment using a transmission cell.

Several X-ray observations of the gap between water and octadecyltrichlorosilane (OTS) SAMs[4−7] have implied effective gap widths D_{eq} of just above 1 Å. For example, three papers by Mezger et al.[4,6,7] report data that translate to D_{eq} = 1.1 Å. The data in Poynor et al.[5] yield slightly higher numbers

Received: December 9, 2019
Revised: December 29, 2019
Published: January 8, 2020

https://dx.doi.org/10.1021/acs.langmuir.9b03785
Langmuir 2020, 36, 906−910

(2−3 Å). In addition to water, molten octadecanol has been reported to show an interfacial gap with a similar D_{eq}.[12] However, Ocko et al[13] have noted that a depletion corresponding to $D_{eq} \sim 1$ Å in our notation is roughly what is expected from the layer of CH_3 groups at the surface of the SAM molecules, which have a lower electron density than CH_2 groups. We can equivalently attribute this depletion to the terminal H atom of each molecule. (Incidentally, water also shows a gap at fluorocarbon SAMs;[7,9,10] these surfaces will not be discussed in this paper.)

Water is of course a crucially important liquid, but it is not the only liquid of interest in real-world applications. Tribology, for example, generally involves organic lubricants. The interactions between molecules and surfaces are complex and include electrostatic forces, van der Waals forces, hydrogen bonding, etc. Is every liquid different, or are there some general features regarding how liquids make contact with hydrophobic surfaces? We have addressed the question by studying the interface profiles between octadecyltrichlorosilane (OTS) self-assembled monolayer (SAM) hydrophobic surfaces and a number of polar and nonpolar molecular liquids using X-ray reflectivity. We will show that extending the studies beyond a single liquid or a single class of liquids gives us a clearer picture of what happens at liquid−SAM interfaces.

EXPERIMENTAL SECTION

Our OTS SAMs were prepared following Wang et al.[14] with a few modifications. We used polished thermal (500−1000 nm thick) silicon oxide. This eliminates coherent scattering from the extra Si−SiO_2 interface that exists in silicon wafers with thin (∼10 Å) native amorphous oxide. The structure of that interface[15] is of absolutely no interest in most studies using Si substrates, but adds unnecessary variable parameters to the data fits that increase the uncertainty in the parameters of actual interest. Our thick oxide substrates facilitate comparison of reflectivity data from one sample to another, unlike Si wafers with native oxide where the Si−SiO_2 interface position and profile may vary from sample to sample.

The samples were mounted to the transmission cell, made of Teflon with Kapton windows, using a Teflon screw. More details of such cells can be found elsewhere.[4−10] About 2 mL of solvent is injected into the transmission cell with a glass syringe. All studies were performed at room temperature. The X-ray reflectivity measurements were performed at Beamline 12BM-B of the Advanced Photon Source. The X-ray energy was 19.5 KeV. The beam was focused to 0.2 × 0.2 mm^2. The transmission geometry is shown to the right side of Figure 1. The data were collected with a Pilatus 100 K area detector. All XRR data are shown in this paper in terms of the magnitude q of the momentum transfer vector ($q \equiv |\vec{K}_f - \vec{K}_i|$, where $\vec{K}_i$ and $\vec{K}_f$ are the incoming and outgoing X-ray wave vectors). The off-specular background was determined from the area detector data by taking the counts in directions shifted + 0.2 and −0.2° from the specular direction and averaging them. These directions are sufficiently far from the specular direction that they represent the uniform background. This background was subtracted from the specular counts.

The quality of the OTS film is key for liquid−solid interface studies. This is especially true for XRR measurements since the X-rays cover a large footprint on the sample, and lateral variations will blur the phenomena of interest. Poynor et al.[5] have found that bad-quality samples show quite different reflectivity patterns from normal samples. Our samples were examined with water contact angle measurements (VCA Optima XE) and had > 115 ± 3° advancing contact angles, in agreement with the literature.[14,16] The reflectivity measurements were also performed on OTS films in contact with air, showing clear oscillations up to 0.84 $Å^{-1}$ (Figure 2, center column, top). Fitting of dry OTS data gave parameters (see Supporting Information) that are in agreement with other published results.[17]

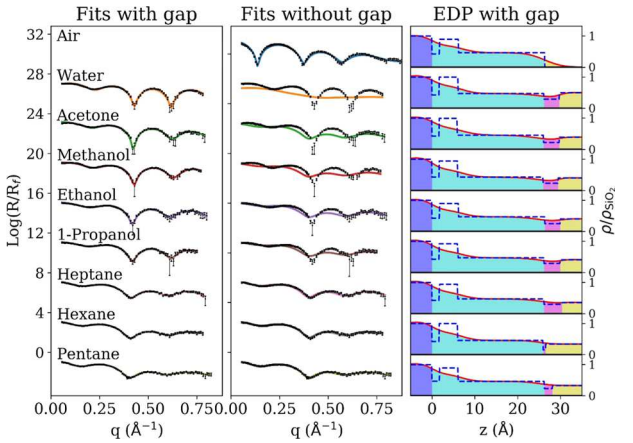

Figure 2. Reflectivity data normalized by the Fresnel reflectivity for the dry OTS film (labeled "air") and OTS films with liquids (labeled with the liquid name). The lines through the data show fits to slab models of the interfacial profiles (Figure 1) LEFT: Best fits including a density-depleted gap layer. MIDDLE: Same data with best fits not including a gap layer. RIGHT: Electron density profiles (EDP) for the gap fits shown in the left panel, i.e., for the fits that include gaps. (The model parameters for these fits can be found in the Supporting Information. Note that for the SAM−air interface, the EDP shown is for the no-gap fit since a gap would be meaningless when there is no liquid.)

For all of the liquids studied, we have fitted the observed X-ray reflectivities from the liquid−SAM interfaces using slab models with (and also without) the gap layer shown in Figure 1. We have then plotted some confidence regions (to be defined and discussed later in the paper) in the plane of gap width (D_g) and gap scattering length density (ρ_g) parameters.

Note that the scattering length density (SLD) is the number of electrons per $Å^3$ multiplied by the classical radius of the electron in angstrom; thus, it is in units of $Å^{-2}$ but is proportional to the electron number density. Therefore, in discussing the qualitative trends in our results, we have used "density", "electron density", and 'scattering length density' interchangeably.

RESULTS AND DISCUSSION

The electron density contrast at an OTS−liquid interface is lower than the contrast at the interface between OTS and air. Thus, the XRR curves are different from the dry OTS curve (see Figure 2). All of the minima shift to higher q values compared to dry OTS. The polar liquids (water, acetone, methanol, ethanol, and 1-propanol) show strong peaks and valleys in the reflectivity, whereas the nonpolar liquids (heptane, hexane, and pentane) have only weak features. This is the essential qualitative difference from which the quantitative findings in this paper follow.

To fit these reflectivity data, the electron density of the OTS SAM/solvent system is modeled as a succession of slabs (Figure 1). The model reflectivity was calculated by Parratt's recursive method. Following Steinrück et al.[15,17] the OTS layer was represented by three slabs: the first slab represents the silane anchor at the substrate; the second slab accounts for the higher density Si−O−Si group, and the third slab represents the hydrocarbon chains. Our silicon substrate has a macroscopic oxide layer and therefore requires only one semi-infinite slab. For the XRR data from OTS−solvent interfaces, a gap

https://dx.doi.org/10.1021/acs.langmuir.9b03785
Langmuir 2020, 36, 906−910

layer was introduced into our fits, as well as a semi-infinite layer of liquid of known electron density. (All these slabs are shown in Figure 1).

Since the SiO_2 layer and liquid layer are semi-infinite and have known electron densities, our model contains the following variable parameters: four slab widths (D_{head1}, D_{head2}, and D_{chain} for the SAM and D_g for the gap), four slab electron densities (ρ_{head1}, ρ_{head2}, ρ_{chain}, and ρ_g), and five interface widths ($\sigma_{Si\text{-}head1}$, $\sigma_{head1\text{-}head2}$, $\sigma_{head2\text{-}chain}$, $\sigma_{chain\text{-}gap}$, $\sigma_{gap\text{-}liquid}$). In each group, the last variable is obviously not used for fits that do not include a gap. We used our own fitting program to vary these parameters and to generate the data for the confidence region plots (discussed further below). The allowed ranges of these parameters were restricted to prevent the software from arriving at unreasonable values. All interface widths were required to be > 1 Å, and SAM layer densities were allowed to vary no more than 15% from the values obtained in a dry-SAM XRR fit.

Fitting of experimental data requires varying model parameters until an appropriate merit function is minimized. Fitting of reflectivity data involves some special considerations.[10,18−20] Because of the strong variation in intensity across the q-range of the reflectivity data, familiar merit functions such as χ^2 will largely ignore the higher-q region where all of the relevant interference effects appear. It is therefore necessary to use merit functions that reduce the dominance of the numerically larger low-q data. The logarithmic merit function that we have used is specified and discussed in the Supporting Information.

Fits were also performed both with and without a gap (Figure 2, center panel) to see if a gap is necessary for a good fit. A slab model with a gap layer (Figure 1) will fit the XRR data from all liquids (Figure 2, left). Without the gap layer (Figure 2, middle), the fitting for the nonpolar liquids pentane and hexane still works perfectly, but not as well for heptane. For all of the polar liquids as well as water, the no-gap fit fails badly—the best-fit reflectivities (solid lines) do not conform to the data. Thus, a gap is essential to fit the polar liquid reflectivity data. Parameters for the best fits in Figure 2 are tabulated in the Supporting Information.

It has been a frequent practice in the reflectivity literature to report only a single set of best-fit parameters as determined by fitting software. In fact, one cannot attribute any unique significance to the single fit corresponding to the global or local minimum of the merit function.[21] This is because the experimental data are not infinitely accurate; if the data points are randomly shifted up or down within the range of their error bars, the best-fit parameters will change as well. This is why we have relegated the best-fit parameters to the Supporting Information and instead emphasize here the parameter ranges that give good fits.

For a discussion of confidence intervals, see, e.g., "The Art of Scientific Computing" by Press et al.[21] They show that in the plane of a fit with two parameters (D_g and ρ_g in our case), the range in parameter space from the lowest value of χ^2 to a value that is higher by 1 (in other words, $\Delta\chi^2 = 1$) covers a 68% confidence region. Other confidence regions can be similarly determined—see ref 21. (Incidentally, the "best fit", in and of itself, would occupy a 0% confidence region.)

Each of the eight contour maps in Figure 3 is constructed from 14,400 (120 × 120) fits to the reflectivity data at equally spaced points across the D_g−ρ_g regions shown. At each point, D_g and ρ_g were fixed, and all other parameters were allowed to vary until the best fit at that point is found. Note that this procedure is quite different from, and more rigorous than, keeping all of the other parameters fixed and simply plotting the nonminimized merit function over the parameter plane, as some canned XRR fitting programs will do. It is also common to determine standard deviations in fitting parameters by starting with an optimized fit and then varying only the parameter whose standard deviation is being determined. While such standard deviations could be called confidence intervals, they are not comparable to our irregularly shaped, nonelliptical confidence intervals (Figure 3), which were determined after minimizing the merit function at each point in the D_g−ρ_g plane by varying all other parameters.

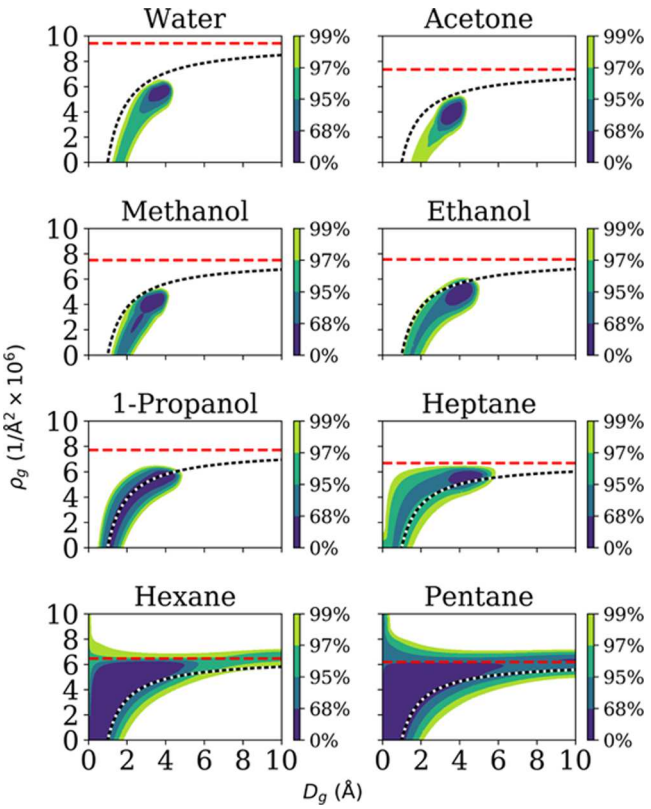

Figure 3. Contour maps showing the 68, 95, 97, and 99% confidence regions for the parameters D_g and ρ_g used in fits to reflectivity data with models that include a gap. The dashed curved line in each plot corresponds to D_{eq} = 1.0 Å. This is a round-number estimate of the electron density depletion due to the terminal H atoms in the SAM;[12] it is not an exact value, and the line is merely a guide to the eye. The red dashed horizontal line corresponds to the bulk liquid electron density: along this line $\rho_g = \rho_L$, and therefore there is no gap. There is also no gap at points along the y-axis because $D_g = 0$ there.

In the Supporting Information, we show some examples of fits through the data at the perimeters of the various confidence regions. Because the experimental data are never infinitely accurate, there is always some probability that a poorer fit is the correct one.

As previously noted, we represent the interfacial density deviations (if any) in terms of gap density ρ_g and gap width D_g only because experimental accuracy does not justify a more complex model. Even so, XRR does not determine a best-fit D_g or ρ_g with great accuracy—the confidence regions do not even have the idealized elliptical shape oriented along the parameter axes from which a mean value and an error estimate for each parameter could be individually determined. Rather, the

https://dx.doi.org/10.1021/acs.langmuir.9b03785
Langmuir 2020, 36, 906−910

regions have irregular shapes: the mean value of ρ_g and its uncertainty depend on the value of D_g and vice versa.

This is illustrated, for example, by the contours for water (top left panel, Figure 3). If we use the 97% confidence region, the range of the scattering length density ρ_g is $0-6 \times 10^{-6}$ Å^{-2}, and the range of D_g is 1.5−4.5 Å; in other words, neither parameter is well defined. On the other hand, D_{eq} (defined above as $D_{eq} \equiv D_g(\rho_L-\rho_g)/\rho_L$, where ρ_L is the electron density of the bulk liquid) is more precisely determined. This was originally pointed out by Mezger et al.[4] and is illustrated in Figure 3 by comparison to the shapes of the dashed curved lines, which connect all D_g and ρ_g values corresponding to D_{eq} = 1 Å. (This gap magnitude is very approximately what is expected due to the layer of terminal H atoms.[13]) It can be seen that the contours have roughly the same shapes as the D_{eq} = 1 Å curve; in other words, the error in D_{eq}, indicated by the lateral widths of the elongated confidence regions, is relatively small. Of course, there is no absolute criterion to tell us which confidence level should be used; thus, some qualitative assessment is required. However, in the present case, the conclusions described below are not significantly dependent on the specific confidence region chosen.

Each panel in Figure 3 contains another guide to the eye: the horizontal dashed line, which is the bulk electron density of the liquid used. When a dark region (low merit function, i.e., excellent fit) reaches this line, it means that the gap has the same density as the bulk liquid, i.e., there is no gap. The same thing is true along the y-axis, where $D_g = 0$.

All five polar liquids, water, acetone ($(CH_3)_2CO$), methanol (CH_3OH), ethanol (CH_3CH_2OH), and 1-propanol ($CH_3(CH_2)_2OH$), show quite similar confidence regions. These regions never include either the horizontal $\rho_g = \rho_L$ lines or the y-axes. For water, acetone, methanol, and ethanol, the confidence regions are to the right of the 1 Å line, with $D_{eq} \approx 1.5 \pm 0.4$ Å using the 99% confidence region. For 1-propanol, the confidence region is roughly symmetric about the 1 Å line, i.e., $D_{eq} \approx 1.0 \pm 0.4$ Å. We conclude that the gap for polar liquids is not strongly dependent on the specific polar liquid used. In other words, it is in large part a property of the substrate, i.e., the terminal H atoms of the SAM, but there is apparently a small additional gap except in the case of propanol. Because of the uncertainties, we cannot make a more unequivocal statement. These data are consistent with published data for water[4−7] and octadecanol.[12]

We see no obvious trends within this group of polar liquids as functions of relative polarity—this varies from 1.0 (water) to 0.36 (acetone), but the gap does not change significantly. (A table of relative polarity values is in the Supporting Information.)

The nonpolar liquids pentane ($CH_3(CH_2)_3CH_3$, the shortest liquid hydrocarbon) and hexane ($CH_3(CH_2)_4CH_3$) are quite different. The confidence regions are much broader and spread out to include the horizontal $\rho_g = \rho_L$ line and the y-axis, where $D_{eq} = 0$. They do also include the D_{eq} = 1 Å line, but parsimony always requires the simpler model, i.e., one with no gap. Gaps are not required to fit the pentane and hexane data, as also illustrated in Figure 2.

Nonpolar heptane ($CH_3(CH_2)_5CH_3$), which is longer, occupies an intermediate position. A gap is required to fit the data (the zero-gap lines are outside our confidence intervals, although only barely). The broad confidence regions are predominantly to the left of and above the 1 Å line, so that $D_{eq} \approx 0.7 \pm 0.6$ Å.

Given that the nonpolar liquids studied are all slightly less dense than the polar liquids, is it possible that the observed gap depends not on whether a liquid is polar or nonpolar but on the electron density of the bulk liquid? If, for example, the gap region happened to have the same density as one of the nonpolar liquids, it would appear to blend in with the bulk liquid; but exactly the same gap region would show up against a denser liquid. However, as emphasized throughout this paper, the gap electron density is not a quantity we can determine with any precision, and thus its density contrast with the bulk liquid is not a well-defined quantity. The reflectivity depends on D_{eq}, which is the effective width of a zero-density gap. Further, we do not see consistent trends as a function of bulk liquid electron density—for example, acetone is less dense than 1-propanol, but has a slightly larger gap (Figure 3).

The magnitude of the gap also has no apparent correlation with the OTS−liquid contact angle. For example, our OTS surfaces show a contact angle of 115 ± 3° with water. Published data[22] show that acetone has a contact angle of 9.5° on OTS, close to that of heptane (<10°). Yet, water and acetone show similar gap contours, whereas heptane is completely different.

CONCLUSIONS

Our data show that polar liquids tend to stand away from the terminal H atoms. Nonpolar liquids, on the other hand, penetrate into the terminal region of the SAM. Smaller-molecule nonpolar liquids thereby entirely obscure the gap, while the longest nonpolar liquid molecule (heptane) only reduces the gap size.

Much of the previous relevant literature on the topic of the interfacial gap[4−10] has been about water. Studying multiple liquids under otherwise identical conditions clarifies the situation considerably. We can now see that for polar liquids, the gap does not depend strongly on the liquid used. Indeed, we find absolutely nothing special about water as far as the gap at a hydrophobic alkane surface is concerned.

Our results might appear to imply that the gap is merely a detail specific to the substrate being used and results from the near-ideal molecular arrangement of the OTS SAM. In fact, however, this idealized arrangement provides us with a sensitive measure of how different liquids interact with other common hydrophobic interfaces. Most hydrophobic surfaces are not as well-ordered as the SAM surface; they will also have H atoms at the surface, but not as many. We suggest that the local environment of each H atom at the surface will still be the same as what we see in OTS monolayers, but the surface-averaged gap size will be smaller. For example, a study of the interfaces between liquid alkanes and water[23] reports that the gap is in the range $D_{eq} \approx 0-0.5$ Å. This is precisely what we would expect based on our own results, given that the liquid alkane surface is disordered and contains fewer exposed H atoms than the more ordered SAM surface.

It is known that water is oriented at hydrophobic interfaces;[11,24,25] it is possible that other polar liquids are oriented also. This may result in a hydrogen-bonded interfacial network that helps keep the liquids away from the solid surface. Nonpolar liquids, on the other hand, are attracted to rather than repelled from the hydrophobic molecules. The result is that polar and nonpolar liquids form quite different interfaces, a finding that is likely to have implications for a tribological response, adhesion, and many other solid−liquid interface processes.

https://dx.doi.org/10.1021/acs.langmuir.9b03785
Langmuir 2020, 36, 906−910

■ ASSOCIATED CONTENT

Supporting Information

The Supporting Information is available free of charge at https://pubs.acs.org/doi/10.1021/acs.langmuir.9b03785.

Fitting parameters for best fits assuming a gap; contact angles and relative polarities; merit function; boundaries of confidence intervals (PDF)

■ AUTHOR INFORMATION

Corresponding Author

Pulak Dutta − *Department of Physics and Astronomy, Northwestern University, Evanston, Illinois 60208-3112, United States;* orcid.org/0000-0002-2111-0546; Email: pdutta@northwestern.edu

Other Authors

Miaoqi Chu − *Department of Physics and Astronomy, Northwestern University, Evanston, Illinois 60208-3112, United States*

Mitchell Miller − *Department of Physics and Astronomy, Northwestern University, Evanston, Illinois 60208-3112, United States;* orcid.org/0000-0001-7266-1092

Complete contact information is available at: https://pubs.acs.org/10.1021/acs.langmuir.9b03785

Notes

The authors declare no competing financial interest.

■ ACKNOWLEDGMENTS

This work was supported by the US National Science Foundation, grant no. DMR-1612876. The X-ray measurements were performed at X-ray Science Division Beamline 12-BM of the Advanced Photon Source, a U.S. Department of Energy (DOE) Office of Science User Facility operated by Argonne National Laboratory under Contract No. DE-AC02-06CH11357.

■ REFERENCES

(1) Chandler, D. Hydrophobicity: two faces of water. *Nature* **2002**, *417*, 491.

(2) Ball, P. How to keep dry in water. *Nature* **2003**, *423*, 25−26.

(3) Chandler, D. Oil on troubled waters. *Nature* **2007**, *445*, 831−832.

(4) Mezger, M.; Reichert, H.; Schöder, S.; Okasinski, J.; Schröder, H.; Dosch, H.; Palms, D.; Ralston, J.; Honkimäki, V. High-resolution in situ x-ray study of the hydrophobic gap at the water−octadecyltrichlorosilane interface. *Proc. Natl. Acad. Sci. U.S.A.* **2006**, *103*, 18401−18404.

(5) Poynor, A.; Hong, L.; Robinson, I. K.; Granick, S.; Zhang, Z.; Fenter, P. A. How Water Meets a Hydrophobic Surface. *Phys. Rev. Lett.* **2006**, *97*, No. 266101.

(6) Mezger, M.; Schöder, S.; Reichert, H.; Schröder, H.; Okasinski, J.; Honkimäki, V.; Ralston, J.; Bilgram, J.; Roth, R.; Dosch, H. Water and ice in contact with octadecyl-trichlorosilane functionalized surfaces: A high resolution x-ray reflectivity study. *J. Chem. Phys.* **2008**, *128*, No. 244705.

(7) Mezger, M.; Sedlmeier, F.; Horinek, D.; Reichert, H.; Pontoni, D.; Dosch, H. On the Origin of the Hydrophobic Water Gap: An X-ray Reflectivity and MD Simulation Study. *J. Am. Chem. Soc.* **2010**, *132*, 6735−6741.

(8) Maccarini, M.; Steitz, R.; Himmelhaus, M.; Fick, J.; Tatur, S.; Wolff, M.; Grunze, M.; Janecek, J.; Netz, R. R. Density depletion at solid-liquid interfaces: a neutron reflectivity study. *Langmuir* **2007**, *23*, 598−608.

(9) Chattopadhyay, S.; Uysal, A.; Stripe, B.; Ha, Y. G.; Marks, T. J.; Karapetrova, E. A.; Dutta, P. How Water Meets a Very Hydrophobic Surface. *Phys. Rev. Lett.* **2010**, *105*, No. 037803.

(10) Uysal, A.; Chu, M.; Stripe, B.; Timalsina, A.; Chattopadhyay, S.; Schlepütz, C. M.; Marks, T. J.; Dutta, P. What X-rays Can Tell Us about the Interfacial Profile of Water near Hydrophobic Surfaces. *Phys Rev. B* **2013**, *88*, No. 035431.

(11) Scatena, L. F.; Brown, M. G.; Richmond, G. Water at Hydrophobic Surfaces: Weak Hydrogen Bonding and Strong Orientation Effects. *Science* **2001**, *292*, 908−913.

(12) Haddad, J.; Steinrück, H.-G.; Hlaing, H.; Kewalramani, S.; Pontoni, D.; Reichert, H.; Murphy, B. M.; Festersen, S.; Runge, B.; Magnussen, O. M.; et al. Order and Melting in Self-Assembled Alkanol Monolayers on Amorphous SiO_2. *J. Phys. Chem. C* **2015**, *119*, 17648−17654.

(13) Ocko, B. M.; Dhinojwala, A.; Daillant, J. Comment on "How Water Meets a Hydrophobic Surface". *Phys. Rev. Lett.* **2008**, *101*, No. 039601.

(14) Wang, Y.; Lieberman, M. Growth of Ultrasmooth Octadecyltrichlorosilane Self-Assembled Monolayers on SiO_2. *Langmuir* **2003**, *19*, 1159−1167.

(15) Steinrück, H.-G.; Schiener, A.; Schindler, T.; Will, J.; Magerl, A.; Konovalov, O.; Destri, G. L.; Seeck, O. H.; Mezger, M.; Haddad, J.; Deutsch, M.; Checco, A.; Ocko, B. M. Nanoscale Structure of Si/SiO2/Organics Interfaces. *ACS Nano* **2014**, *8*, 12676−12681.

(16) Jiang, P.; Li, S.-Y.; Sugimura, H.; Takai, O. Pattern design in large area using octadecyltrichlorosilane self-assembled monolayers as resist material. *Appl. Surf. Sci.* **2006**, *252*, 4230−4235.

(17) Steinrück, H.-G.; Will, J.; Magerl, A.; Ocko, B. M. Structure of N-Alkyltrichlorosilane Monolayers on Si(100)/SiO2. *Langmuir* **2015**, *31*, 11774−11780.

(18) Danauskas, S. M.; Li, D.; Meron, M.; Lin, B.; Lee, K. Y. C. Stochastic fitting of specular X-ray reflectivity data using StochFit. *J. Appl. Crystallogr.* **2008**, *41*, 1187−1193.

(19) Kunz, K.; Reiter, J.; Goetzelmann, A.; Stamm, M. Model-free analysis of neutron reflectivity data from polymer thin films with the simulated annealing technique. *Macromolecules* **1993**, *26*, 4316−4323.

(20) Poloucek, P.; Pietsch, U.; Geue, T.; Symietz, C.; Brezesinski, G. *J. Phys. D: Appl. Phys.* **2001**, *34*, 450−458.

(21) Press, W. H.; Teukolsky, S. A.; Vetterling, W. T.; Flannery, B. P. *Numerical Recipes: The Art of Scientific Computing*; Cambridge University Press, 2007.

(22) Janssen, D.; de Palma, R.; Verlakk, S.; Heremans, P.; Dehaen, W. Static solvent contact angle measurements, surface free energy and wettability determination of various self-assembled monolayers on silicon dioxide. *Thin Solid Films* **2006**, *515*, 1433−1438.

(23) Fukuto, M.; Ocko, B. M.; Bonthuis, D. J.; Netz, R. R.; Steinrück, H.-G.; Pontoni, D.; Kuzmenko, I.; Haddad, J.; Deutsch, M. Nanoscale Structure of the Oil-Water Interface. *Phys. Rev. Lett.* **2016**, *117*, No. 256102.

(24) Du, Q.; Freysz, E.; Shen, Y. R. Surface Vibrational Spectroscopic Studies of Hydrogen Bonding and Hydrophobicity. *Science* **1994**, *264*, 826−828.

(25) Sato, T.; Sasaki, T.; Ohnuki, J.; Umezawa, K.; Takano, M. Hydrophobic Surface Enhances Electrostatic Interaction in Water. *Phys. Rev. Lett.* **2018**, *121*, No. 206002.